

MAGNETISM IN THE INTERFACES OF THE SANDWICHED $\text{PbTiO}_3/\text{LaAlO}_3/\text{SrTiO}_3$ HETERO-STRUCTURE

BACH HUONG GIANG, NGUYEN THUY TRANG, TRAN VAN NAM,
AND BACH THANH CONG

*Computational Material Science Lab, Faculty of Physics, Hanoi University of Science,
Vietnam National University, 334 Nguyen Trai, Thanh Xuan, Hanoi, Vietnam*

E-mail: gianghuongbach@gmail.com

Received 05 September 2014

Accepted for publication 24 April 2015

Abstract. *We investigate the effect of PbTiO_3 on the $\text{LaAlO}_3/\text{SrTiO}_3$ hetero-structure by density functional theory, where the asymmetry sandwich not only forms a quasi-two dimensional electron gas but also reveals a ferromagnetic state in the TiO_2 interfaces. It is found out that magnetic moments of TiO_2 interface layers are around $0.18 \mu_B$ while they are mostly negligible in the pure $\text{LaAlO}_3/\text{SrTiO}_3$ system. Even though magnetic moments are mainly produced by Ti t_{2g} orbitals, oxygen plays a key role in the formation of the ferromagnetic state since polar distortions primarily occur in oxygen positions of the SrTiO_3 and PbTiO_3 sides in opposite directions.*

Keywords: magnetism, $\text{LaAlO}_3/\text{SrTiO}_3$, $\text{PbTiO}_3/\text{LaAlO}_3/\text{SrTiO}_3$.

I. INTRODUCTION

The interface between perovskite structure material has recently exposed various interesting properties, which are completely different than the bulk systems. While LaAlO_3 (LAO) and SrTiO_3 (STO) bulks are both well-known as insulators, an existence of metallic phase has been found on LAO/STO interface. Whether termination layer is SrO or TiO_2 , the interface will be insulator or metal with an extremely high mobility [1]. It is generally believed that free carriers are injected in the interface in order to overcome the “polar catastrophe” [2,3] causing by the polar discontinuity between two perovskites. In addition, a ferromagnetic order and a superconductivity-like phase has been observed co-existentally under a specific temperature and a pressure condition [4], which promisingly brings other clues for understanding the unconventional superconductivity problem. Furthermore, the LAO/STO hetero-structures have a great potential in developing new electronic devices where the conducting gas is controlled by an electric field [5] or by a ferroelectric polarization layer [6,7].

The co-existence of magnetism and conductivity in the LAO/STO interfaces attracts a lot of attentions due to the unrevealed mechanism beneath. In the stoichiometric structures, the conductivity is mostly explained by transferring electrons from the LAO slab to the STO slab if the LAO thickness reaches an critical value $d_c = 4$ unit cells (u. cs) [5]. Even though Ti d-orbitals are

responsible for both magnetism and conductivity, the mechanism of magnetism is still in debates. It has been shown that there can be two reasons to arise a magnetic phase in the STO layers, which are due to the oxygen vacancies [8] or the on-site Coulomb interaction in the Ti d-orbitals [9].

In this paper, we make an attempt to study a sandwiched $\text{PbTiO}_3/\text{LaAlO}_3/\text{SrTiO}_3$ (PLS) by density functional calculations, where an quasi two-dimensional free electron gas has aligned magnetically in all TiO_2 layers. Unlike the stoichiometric structure, free electron gas is formed by chemical doping in this non-stoichiometric PLS. While the magnetic moments is mostly negligible in both LAO/STO stoichiometric and non-stoichiometric structures without using LDA+U calculations, magnetic moments around $0.18 \mu_B$ have been observed in the TiO_2 layers due to the geometric asymmetry of the sandwich. Even though magnetic moments are mainly produced by Ti d-orbitals, the oxygen play a key role in the formation of the ferromagnetic state since polar distortions primarily occur in the oxygen positions of the STO and PbTiO_3 (PTO) slabs in the opposite directions.

II. CALCULATIONAL DETAILS

Ab initio total energy pseudo-potential calculations are carried out using CASTEP (Cambridge Serial Total Energy Package of Accelrys Inc.). The wave functions of valence electrons are expanded in a basis set of plane waves with kinetic energy smaller than a specified cut-off energy. Exchange correlation functional is adopted in the generalized gradient approximations (GGA) parametrized by Perdew and Wang (PW91) [10]. The interaction between valence electrons and ion cores is described by an ultra-soft pseudo-potential. In the process of setting up the CASTEP run, basic parameters are chosen as follows: the cut-off energy is set to be 340 eV; the Brillouin-zone integration is performed using $6 \times 6 \times 1$ k-point sampling, which is generated by the Monkhorst-Pack scheme; fast Fourier transform (FFT) grid dimensions are $24 \times 24 \times 200$ and self-consistent field tolerance is 10^{-6} eV/atom. An optimization using Broyden Fletcher Goldfarb Shanno (BFGS) technique has been performed to speed up the calculation [11]. The structure has been relaxed until the residual forces converged to 0.03 eV/Å and the maximum energy reached below 10^{-5} eV/atom. Since we are interested in the electronic properties of a sandwiched PTO/LAO/STO (PLS) hetero-structure, we construct a slab including 4 LAO u.c. sandwiched by 1 STO u.c. and 1 PTO u.c. (see Fig. 1). These slabs are separated by a 10-Å-thick vacuum to avoid slab-slab interactions. These following calculations are carried out with spin-polarization considerations.

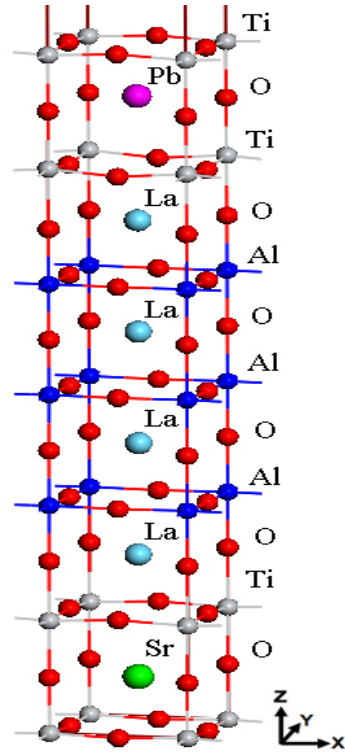


Fig. 1. Atomic structure of the $\text{PbTiO}_3/\text{LaAlO}_3/\text{SrTiO}_3$ slab in which two surfaces are connected to the vacuum.

III. RESULTS AND DISCUSSIONS

A. Polar distortions

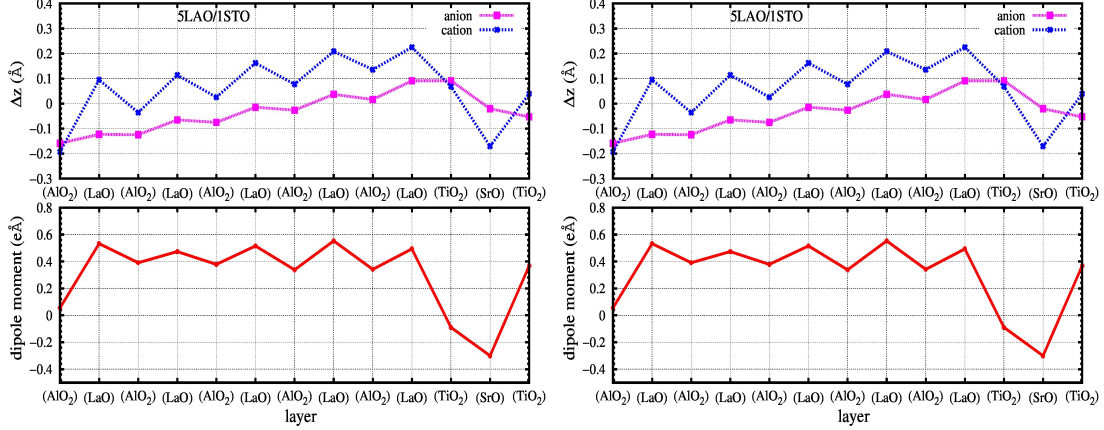


Fig. 2. The cation (anion) displacement along c-axis (top panel) and the layer dipole moment (down panel) for a 5LAO/1STO super cell (left) and for a 1PTO/4LAO/1STO super cell (right).

In order to comprehend the PTO cell effects on the 4LAO/STO hetero-structure, we compare the electronic structures of the 5LAO/1STO and the 1PTO/4LAO/1STO supercells after carrying out the relaxation process. Since the translational symmetry is broken at the interface, the structures are reconstructed to minimize structural energy, resulting in the polar distortions. Fig. 2 shows a displacement from initial positions before doing relaxation along c-axis of cations (anions) in each layers for the 5LAO/1STO cell (left) and for the 1PTO/4LAO/1STO cell (right). For the 5LAO/1STO cell, O atoms in the LAO side move inwardly to the surface whereas La and Al atoms moves outwardly, which creates a dipole moment in each layer. The dipole moment presented in the bottom panel of Fig. 2 is approximately calculated from the cation (anion) displacement in c-axis, Δz , by this relation [12]:

$$P = \sum_i Z_i \Delta z_i \quad (1)$$

where P is the layer dipole moment, Z is the formal atomic charge and the sum is taken over all atoms of each layer. It is clearly seen that strong dipole moments of LaO layers (0.58 eÅ) and AlO_2 layers (0.38 eÅ) are arisen in the 5LAO/1STO case, which agrees well with Ref. [12, Fig. 2]. The dipole moment of TiO_2 interface is negligibly small (0.08 eÅ). The total dipole moment calculated by summing all layers's dipole moments are respectively 4.07 eÅ , -0.02 eÅ for the LAO and STO slabs. For the 1PTO/4LAO/1STO case, the cation and anion roughly relax the same amount so that the dipole moments of the LAO side (0.08 eÅ) strongly reduces in comparison with that in the 5LAO/1STO. While those dipole moments are mostly uniform in all layers of LAO sides, the dipole moment of the STO/ TiO_2 interface behaves differently, in which P increases to -0.4 eÅ . The dipole moment of the PTO/ TiO_2 interface enhances even stronger, around 0.72 eÅ . The dipole moment observed in the 1PTO/4LAO/1STO case behaves similarly to the super-lattice structure,

where the polar distortion occurs mostly in the STO side instead of buckling in the LAO side for the 5LAO/1STO case [3]. The total dipole moments are $0.58 \text{ e}\text{\AA}$, $0.83 \text{ e}\text{\AA}$, $-0.51 \text{ e}\text{\AA}$ for the PTO, LAO and STO slabs respectively, which are much smaller compared with that in the 5LAO/STO case. It is clearly seen that the dipole moment is reduced with the increase of LAO thickness, which gives rise to the two-dimensional free electron gas, but does not occur in the PLS case.

B. Partial density of states and magnetic moments

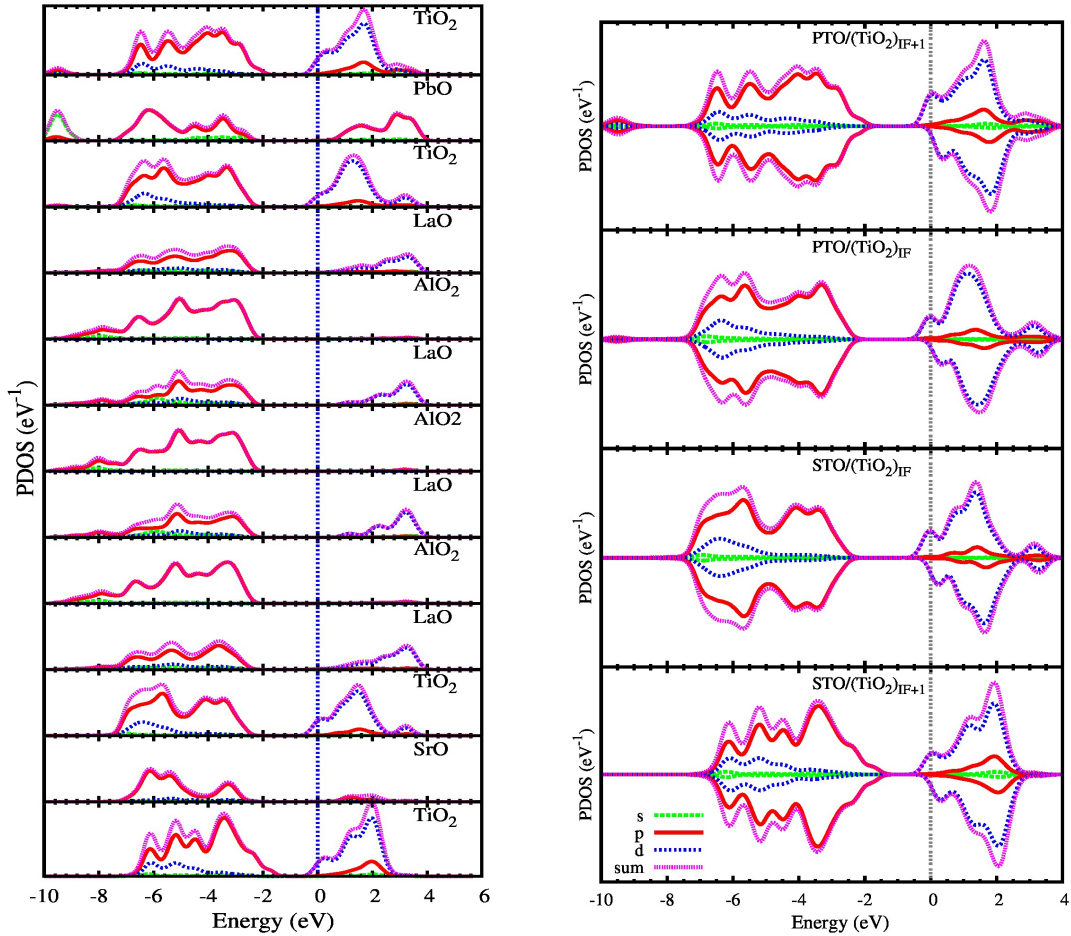


Fig. 3. (a) Layer-projected partial density of states in a PLS unit cell (left) and (b) the partial density of state of the TiO_2 layers for two spin channels (right). Note that $\text{PTO}/(\text{TiO}_2)\text{IF}$ ($\text{STO}/(\text{TiO}_2)\text{IF}$) denotes TiO_2 layer at the PTO/LAO (STO/LAO) interface and $(\text{TiO}_2)\text{IF}+1$ denotes the next TiO_2 layer from the interface.

Layer-projected partial density of states of TiO_2 layers are plotted in Fig. 3a for the PLS case. A Fermi level crossing the conduction band in the TiO_2 layers exhibits the existence of free electron gas in these layers. While the valence bands close to the Fermi energy are mostly formed

by the O p-band, the conduction bands mostly are composed of the Ti d-band. The gaps in each TiO_2 layers are originated from the bonding and anti-bonding gaps between O p-orbitals and Ti-d orbitals. The most surprising thing is that the band structure shows an existence of magnetic moments in this structure, which is barely found in the LAO/STO hetero-structure without a LDA+U calculation. Fig. 3b presents a splitting partial density of states (PDOS) for each spin, where the up-panel (downpanel) corresponds to PDOS for spin-up (spin-down). The magnetic moments and number fillings of the TiO_2 layers are calculated in TABLE 1. The existence of magnetic moments in all TiO_2 layers can be originated from the asymmetry of Pb and Sr in the PLS structure. Firstly, we can see that in Fig. 3a, the Pb s-orbital contributes a small density around -9.8 eV in the DOS of the PbO layer while SrO shows no contribution at that energy. Since Pb hybridizes not only with O in the PbO layer but with O in the adjacent TiO_2 layers as well, this peak at -9.8 eV are also observed in TiO_2 layers. Secondly, TiO_2 conduction bands exhibit different splittings in every layers, which proves the inhomogeneity through the z-direction. It has been known that, the d-orbital in the octahedral crystal field is split into triply-degenerate t_{2g} (dx_y, dy_z, dz_x) with low energy and doubly-degenerate e_g (dx^2-y^2, dz^2) with high energy. Meanwhile t_{2g} are non-bonding states, e_g are bonding states which easily combine with the O p-orbitals to form bonding and anti-bonding states. An orbital analysis shows that the valance bands corresponding to bonding states include mostly O p-orbitals and slightly Ti e_g orbitals (Fig. 3b). Conduction bands are formed by anti-bonding states including mostly Ti e_g orbitals and non-bonding orbitals, t_{2g} . The polar distortions in the STO and PTO slabs reduce the symmetry of the TiO_6 octahedron, which decides a splitting gap Δ between e_g and t_{2g} , hence, determines the position of bonding-anti-bonding gaps and the overlaps between non-bonding states (t_{2g}) and anti-bonding states (e_g). In this case, two Ti-O bond lengths in the z-direction of the octahedron TiO_6 are shorter than those in the xy plane (see Fig. 2). The compression of the octahedral crystal field splits t_{2g} into a lower d_{xy} and doubly-degenerate dy_z, dz_x so that the system obtains benefits from lowering energy for Ti d^1 configuration [13]. In fact, an orbital analysis shows the most contribution of the conduction band obtained from d_{xy} orbital.

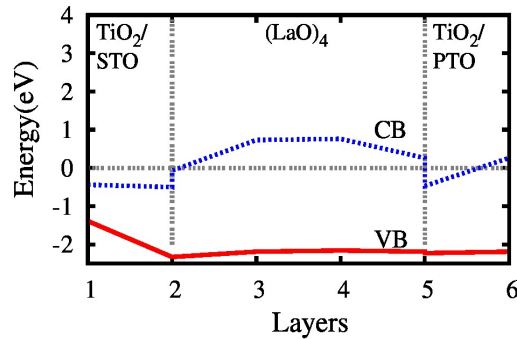


Fig. 4. The top of the valence band and the bottom of the conduction band of TiO_2 and LaO layers.

Fig. 4 obtains the top of the valence band and the bottom of the conduction band of the TiO_2 and LaO layers, which describes the asymmetry between STO and PTO slabs. The fact that

the total dipole moments of STO slabs ($-0.51 \text{ e}\text{\AA}$) is opposite direction with the ones of LAO and PTO slabs ($0.83 \text{ e}\text{\AA}$ and $0.58 \text{ e}\text{\AA}$) gives rise to the layer-dependence of the valence band edge in the STO slab in contrast to flat valence band edges in the LAO and STO slabs. The flat valence band shape has been observed in the extrinsic doping, for example in the case of oxygen vacancies, where the polar field is completely compensated [14]. A band bending for the conduction band edges determines the carrier densities and their mobilities. We can see that, the number of the carrier densities is concentrated mainly in the TiO₂ interface of the STO slabs and reduces in the second layer while it occurs in the opposite way in the PTO slab (see Table 1). This observation implies that a free electron gas may be confined in the quasi two dimensions of the STO slab while the PTO may create an three dimensional electron gas. Therefore, PTO can be used to control the two-dimensional gas between STO/LAO interface by switching an polarization of the PTO slab under electric field [7].

Table 1. Magnetic moments and filling numbers of TiO₂ Layers.

Layer position	Magnetic moment (μ_B)	Filling number	Carrier density (cm^{-2})
STO/(TiO ₂) _{IF}	0.18	0.29	1.95×10^{14}
STO/(TiO ₂) _{IF+1}	0.11	0.19	1.26×10^{14}
PTO/(TiO ₂) _{IF}	0.17	0.22	1.43×10^{14}
PTO/(TiO ₂) _{IF+1}	0.22	0.26	1.74×10^{14}

IV. CONCLUSION

The effect of the PTO slab on the LAO/STO heterostructure is investigated by density functional theory, which is motivated from the ability of controlling the two-dimensional gas in the LAO/STO interface through the PTO slab. A quasi two-dimensional electron gas is aligned ferromagnetically in the LAO/STO interface without using LDA+U. It has been observed that both the magnetic moment and the carrier density are enhanced in the TiO₂ interface (LAO/STO) and reduce in the second TiO₂ layer. The formation of magnetic moments occur mostly in the Ti d-band as a consequence of polar distortions due to breaking translational symmetry along z -direction. The contraction of the octahedron TiO₆ normally split d-band to lower degeneracy, which often favors a ferromagnetic order for Ti d¹ configuration.

ACKNOWLEDGMENT

The authors would like to thank Dr. Nguyen Van Lien and Dr. Vu Thanh Tra for their useful discussions. This research is funded by Vietnam National Foundation for Science and Technology Development (NAFOSTED) under grant number 103.02-2012.73 and by QG12.01

REFERENCES

- [1] A. Ohtomo and H. Hwang, *Nature* **427** (6973) (2004) 423–426.
- [2] K. Yoshimatsu, R. Yasuhara, H. Kumigashira, and M. Oshima, *Phys. Rev. Lett.* **101** (2) (2008) 026802.
- [3] K. Yoshimatsu, R. Yasuhara, H. Kumigashira, and M. Oshima, *Phys. Rev. Lett.* **101** (2) (2008) 026802.

- [4] X. Wang, G. Baskaran, Z. Liu, J. Huijben, J. Yi, A. Annadi, A. R. Barman, A. Rusydi, S. Dhar, Y. Feng, et al., *Nature Communications* **2** (2011) 188.
- [5] S. Thiel, G. Hammerl, A. Schmehl, C. Schneider, and J. Mannhart, *Science* **313** (5795) (2006) 1942–1945.
- [6] C. Bark, P. Sharma, Y. Wang, S. H. Baek, S. Lee, S. Ryu, C. Folkman, T. R. Paudel, A. Kumar, S. V. Kalinin, et al., *Nano Letters* **12** (4) (2012) 1765–1771.
- [7] V. T. Tra, J.-W. Chen, P.-C. Huang, B.-C. Huang, Y. Cao, C.-H. Yeh, H.-J. Liu, E. A. Eliseev, A. N. Morozovska, J.-Y. Lin, et al., *Advanced Materials* **25** (24) (2013) 3357–3364.
- [8] N. Pavlenko, T. Kopp, E. Y. Tsymbal, G. Sawatzky, and J. Mannhart, *Phys. Rev. B* **85** (2) (2012) 020407.
- [9] K. Janicka, J. P. Velez, and E. Y. Tsymbal, *Journal of Applied Physics* **103** (7) (2008) 07B508.
- [10] J. P. Perdew and Y. Wang, *Phys. Rev. B* **45** (23) (1992) 13244.
- [11] B. G. Pfrommer, M. Côté, S. G. Louie, and M. L. Cohen, *Journal of Computational Physics* **131** (1) (1997) 233–240.
- [12] R. Pentcheva and W. E. Pickett, *Phys. Rev. Lett.* **102** (10) (2009) 107602.
- [13] R. Janes and E. A. Moore, *Metal-ligand bonding*, The Open University, Royal Society of Chemistry, 2004.
- [14] Y. Li, S. N. Phattalung, S. Limpijumnong, J. Kim, and J. Yu, *Phys. Rev. B* **84** (24) (2011) 245307.